

17. Pálsson, G. & Kotliar, G. Thermoelectric response near the density driven Mott transition. *Phys. Rev. Lett.* **80**, 4775–4778 (1998).
18. Grimvall, G. *The Electron-Phonon Interaction in Metals* 212 (North-Holland, Amsterdam, 1981).
19. Gelfand, M. P. & Lu, J. P. Orientational disorder and normal-state electrical-transport properties of A_3C_{60} . *Phys. Rev. B* **46**, 4367–4370 (1992).
20. Allen, P. B. & Silbergliitt, R. Some effects of phonon dynamics on electron lifetime, mass renormalization, and superconducting transition temperature. *Phys. Rev. B* **9**, 4733–4741 (1974).

Acknowledgements

We are grateful to M. Jarrell for making his MaxEnt program available and E. Koch for a careful reading of the manuscript. The work has been supported by the Max-Planck-Forschungspreis.

Correspondence and requests for materials should be addressed to O.G. (e-mail: gunnar@and.mpi-stuttgart.mpg.de).

Collapse of stiff conjugated polymers with chemical defects into ordered, cylindrical conformations

Dehong Hu*, Ji Yu*, Kim Wong*, Biman Bagchi†, Peter J. Rossky* & Paul F. Barbara*

* Department of Chemistry & Biochemistry, University of Texas, Austin, Texas 78712, USA

† Solid State and Structural Chemistry Unit, Indian Institute of Science, Bangalore 560012, India

The optical, electronic and mechanical properties of synthetic and biological materials consisting of polymer chains depend sensitively on the conformation adopted by these chains. The range of conformations available to such systems has accordingly been of intense fundamental^{1,2} as well as practical^{3–6} interest, and distinct conformational classes have been predicted, depending on the stiffness of the polymer chains and the strength of attractive interactions between segments within a chain^{7–10}. For example, flexible polymers should adopt highly disordered conformations

resembling either a random coil or, in the presence of strong intrachain attractions, a so-called ‘molten globule’^{2,10}. Stiff polymers with strong intrachain interactions, in contrast, are expected to collapse into conformations with long-range order, in the shape of toroids or rod-like structures^{8,9,11}. Here we use computer simulations to show that the anisotropy distribution obtained from polarization spectroscopy measurements on individual poly[2-methoxy-5-(2'-ethylhexyl)oxy-1,4-phenylenevinylene] polymer molecules is consistent with this prototypical stiff conjugated polymer adopting a highly ordered, collapsed conformation that cannot be correlated with ideal toroid or rod structures. We find that the presence of so-called ‘tetrahedral chemical defects’, where conjugated carbon–carbon links are replaced by tetrahedral links, divides the polymer chain into structurally identifiable quasi-straight segments that allow the molecule to adopt cylindrical conformations. Indeed, highly ordered, cylindrical conformations may be a critical factor in dictating the extraordinary photophysical properties of conjugated polymers, including highly efficient intramolecular energy transfer and significant local optical anisotropy in thin films.

Figure 1 illustrates a range of possible conformations that can be adopted by polymer chains. To investigate the conformational properties of poly[2-methoxy-5-(2'-ethylhexyl)oxy-1,4-phenylenevinylene] (MEH-PPV), a widely studied prototype of stiff conjugated polymers, we use a single-molecule spectroscopy approach^{12–15} and MEH-PPV samples that have an average molecular weight of 453,000 with 1,700 repeat units in a typical polymer molecule¹⁶. As a result of conformational distortions^{17,18}, chemical defects along the polymer chain¹⁹, and electron correlation effects²⁰, the lowest-energy optical absorption of an isolated MEH-PPV molecule is due to about 140 different local ‘quasi-chromophores’ along the chain, each with a length of 10–17 repeat units²¹. For each chromophore, the $\pi-\pi^*$ absorption is polarized along the direction of the local segment of the chain²². Although there is a distribution of repeat-unit lengths and spectroscopic transition energies, the optical transitions are overlapped near the absorption peak (~ 500 nm) due to vibronic broadening²³. There is convincing evidence that the majority of the emission actually occurs from a small region on the polymer chain, due to rapid and efficient intramolecular electronic energy transfer^{16,19}.



Figure 1 Typical conformations of a 100-segment homopolymer generated by Monte Carlo simulations. The simulation parameters are summarized in Table 1. They are

denoted as: **I**, random coil; **II**, molten globule; **III**, toroid; **IV**, rod; **V**, defect-coil; and **VI**, defect-cylinder.

The MEH-PPV molecules are isolated at low concentration in 300-nm-thick, spin-coated inert polymer film (typically polycarbonate) on a glass cover-slip substrate. The MEH-PPV molecules are laterally separated in the film plane (denoted by $x-y$) of the sample on average by $3\ \mu\text{m}$. Individual molecules are optically excited with focused (spot size $\sim 400\ \text{nm}$), linearly polarized light propagating in the z direction using an oil immersion objective located on the substrate side of the sample. The MEH-PPV emission is collected along the z direction with the same objective used for excitation, filtered to remove scattered excitation light, and detected with an avalanche photodiode detector, all with a minimal bias for polarization. The direction of polarization, θ , of the excitation light is linearly temporally modulated between 0 and π with a period of one second by an electro-optic modulator²⁴. The total unpolarized fluorescence intensity, $I(\theta)$, is synchronously recorded for 30 cycles of the modulation, corresponding to 10^7 excitations of MEH-PPV.

$I(\theta)$ is observed to be invariant with cycle within experimental error during this averaging process for the vast majority of the MEH-PPV molecules. Time- and wavelength-resolved spectroscopy of individual polymer molecules demonstrates that $I(\theta)$ is not distorted by spectral diffusion, blinking or other photo-induced processes. The invariance of $I(\theta)$ implies that the characteristic chain conformation of each molecule is fixed on the experimental timescale. A typical averaged $I(\theta)$ is shown as the inset in Fig. 2. It is important to emphasize that $I(\theta)$ reports the polarization dependence of the excitation (absorption) process through the emission intensity. The quasi-chromophore can be approximated by a transition dipole along the local direction of the polymer chain²², so that the absorption is due to a set of about 140 comparable transition dipoles, each oriented along a particular direction in the $x-y-z$ laboratory coordinate system. The corresponding absorption properties of a single polymer molecule can be represented by an ‘‘absorption ellipsoid’’ in the molecular frame (x', y', z') with three distinct orthogonal absorption cross-sections²⁵: C_x , C_y , and C_z . $I(\theta)$ is the projection of this absorption ellipsoid in the $x-y$ plane, as the propagation direction is along z . The functional form of $I(\theta)$ is thus

$$I(\theta) \propto 1 + M \cos 2(\theta - \phi) \quad (1)$$

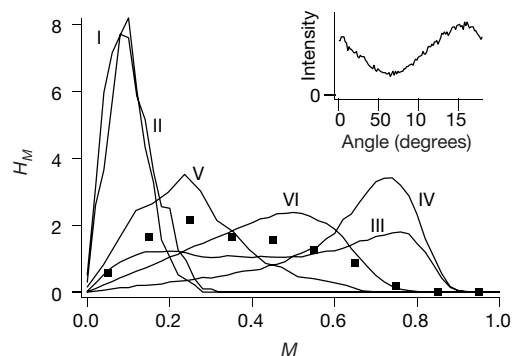


Figure 2 The distribution H_M of modulation depths M from single-molecule polarization spectroscopy and from Monte Carlo simulations. The squares show the distribution for 102 MEH-PPV single molecules measured from polarized fluorescence excitation intensity. The lines are the simulated distributions for the six polymer conformational types, shown in Fig. 1. The simulation parameters are given in Table 1. Inset, $I(\theta)$ for a single MEH-PPV molecule. The film was prepared by spin coating from a toluene solution. Oxygen was excluded from the film by outgassing under vacuum and coating with a 200-nm Al layer. Samples (ambient temperature) were excited at 488 nm using a numerical aperture of 0.7 and a laser power of 50 nW. Emission was collected with a numerical aperture of 1.25.

where the modulation depth M is the anisotropy of the absorption ellipsoid projected on the $x-y$ plane, and ϕ is the orientation of maximum absorption. Our experimental $I(\theta)$ (inset in Fig. 2) is well fitted by equation (1). The observed ϕ values are randomly distributed between 0 and π , as expected.

To determine the absorption ellipsoid for a specific polymer chain, it would be necessary to make measurements with light propagation along multiple axes. However, this is not possible with our apparatus. We rely instead on the distribution of molecular orientations of the entire polymer molecule to achieve this goal. We record M for a large number of single molecules and construct a histogram of M values (H_M as shown in Fig. 2.) The ensemble of values of the single polymer molecule property M reflects the distribution of chain orientations, chain conformations, and molecular weights. The physical significance of H_M can be established by considering limiting cases. For a straight polymer chain, the individual transition dipoles fall on a straight line, and H_M is a delta function located at $M = 1$. In the opposite limit, that is, a perfectly isotropic distribution of dipoles (for example, a random coil of infinite chain length) the absorption ellipsoid is a sphere, and H_M is a delta function located at $M = 0$. We have experimentally verified the latter case by studying approximately 10^4 randomly oriented dye molecules embedded in a 100-nm latex sphere. Those data demonstrate that there is an experimental error of about 0.1 in the M axis of Fig. 2.

We have used Monte Carlo simulation of beads on a chain (bond fluctuation method^{26,27}) to generate an ensemble of conformations for model polymer chains with different numbers of chain defects, intersegment attraction, and chain stiffness. An individual bead or segment represents a small portion of the polymer chain, that is, 2.5 repeat units, which corresponds to 1.5 nm. Typically, a chain with 100 beads was used in the simulations representing a MEH-PPV molecule with 250 repeat units. (Simulations with more beads were prohibitively time-consuming.) The intrachain interactions were modelled with a Lennard-Jones-like attractive potential between a pair of beads with depth E_{cc} . Simulations with a square-well intersegment potential gave analogous results. The chain bending energy $E_{\text{bend}} = b\alpha^2$, where α is the bending angle. The equilibrium bond angle between adjacent bonds was assumed to be 180° except in the case of defects, which are discussed below. The bending force constant, b , was estimated from published force fields for solid polymer²⁸. We note that the intrachain interaction model gives a differential free energy for the polymer in a solvent, arising in part

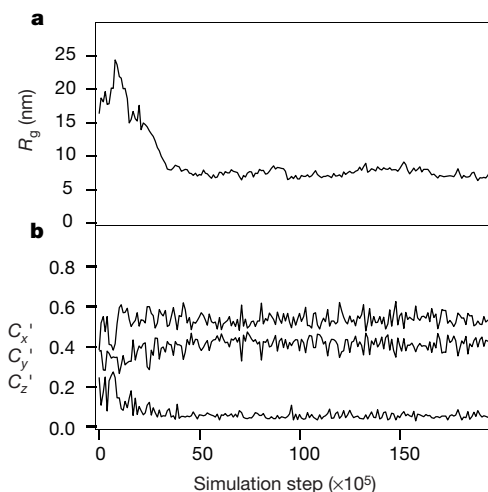


Figure 3 The structural collapse trajectory of a random coil to a toroid. **a**, The radius of gyration R_g ; and **b**, the normalized absorption cross-sections along the three principal axes of the conformation are plotted versus Monte Carlo simulation steps.

Table 1 Conformations and simulation parameters of homopolymers

Symbol	Type	E_{cc}^* (kT)	b (kT rad ⁻²)	Number of defects	$\langle M^2 \rangle^{1/2} \dagger$	$\langle R_g^2 \rangle^{1/2} \ddagger$ (nm)
I	Random coil	0	0	N/A	0.11	13
II	Molten globule	0.6	0	N/A	0.12	5.0
III	Toroid	0.6	10	0	0.53	7.4
IV	Rod§	0.6	10	0	0.67	10
V	Defect-coil	0	10	15	0.28	21
VI	Defect-cylinder	0.6	10	15	0.46	7.2

All simulations were conducted on the same cubic three-dimensional lattice. The lattice constant is 0.3 nm. The linked bead distance is restricted from 1.2 nm to 1.8 nm (4 to 6 lattice units). The bead displacement is one lattice unit. The simulations are usually conducted for 10⁸ Monte Carlo steps. A fixed number of defects are at random locations of the chain. Harmonic bending potential: $E_{bend} = b\alpha^2$. N/A, not applicable.

* E_{cc} is the depth of a Lennard-Jones attraction potential between bead pairs of the polymer chain. The bead attraction potential is:

$$E_{LJ} = \begin{cases} \infty & \text{if } l \leq 2.1 \text{ nm} \\ 4E_{cc} \left(\left(\frac{2.1}{l} \right)^{12} - \left(\frac{2.1}{l} \right)^6 \right) & \text{if } 2.1 \text{ nm} < l \leq 4.2 \text{ nm} \\ 0 & \text{if } l > 4.2 \text{ nm} \end{cases}$$

† $\langle M^2 \rangle^{1/2}$ is the root mean square of the modulation depth of anisotropy.

‡ $\langle R_g^2 \rangle^{1/2}$ is the root mean square of radius of gyration.

§ Rods composed of two to six straight-chain regions are observed in the simulations. R_g strongly depends upon the number of straight-chain regions in a rod and the distribution among types of rods is not converged in our limited number of simulations (20 trials). To avoid this source of error in Table 1, we restrict our analysis of R_g and M to rods with four straight-chain regions.

|| This number corresponds to 15 defects per polymer chain of 100 beads. Since the stiffness parameter (b) has been chosen such that each bead represents 2.5 repeat units, a polymer chain with 15 defects actually corresponds to 6% of the underlying 250 units.

from the difference between interactions among polymer segments compared to polymer with solvent. In general, this free energy will be dependent on solute conformation. For a polymeric solvent, as exists in the present films, one might expect this dependence to be more significant than for a simple solvent, due to the conformational coupling of solvent and solute. This additional complexity is not captured in the highly simplified polymer models used in the present investigation.

For each parameter set, an ensemble of 20 chain conformations was generated. Each conformation is from a distinct initial conformation after about 10⁸ Monte Carlo steps (one step is one attempted move for each bead of the chain). The set of conformations were used to calculate the ensemble averaged: radius of gyration, R_g ; laboratory frame anisotropy (or modulation depth), M (Table 1); and H_M . For the anisotropy calculations, it was assumed that each local transition dipole was along the bond connecting the adjacent beads.

The simplest example we consider is the flexible chain ($b = 0$) with no attraction ($E_{cc} = 0$), which adopts the well known self-avoiding random-coil conformation. A typical example of a random-coil conformation from the simulation is shown in Fig. 1, structure I. The random coil conformation has an H_M distribution (curve I in Fig. 2) that is considerably less anisotropic than the experimental results. The average anisotropy of 0.11 (Table 1) is consistent with theory for the random coil, predicting that $\langle M^2 \rangle^{1/2} \propto N^{-1/2}$ where $N+1$ is the number of beads²⁹. It is well established^{1,2} that chain-chain attraction of sufficient magnitude will induce a flexible chain to collapse to a compact conformation. A typical molten-globule conformation from the simulations ($E_{cc} = 0.6$ kT, $b = 0$) is shown by structure II in Fig. 1. The H_M curve for the molten globule is similar to that for the random coil, reflecting the “liquid-like” disorder in the globule¹⁰, but the radius of gyration is smaller for the molten globule (Table 1).

The inclusion of chain stiffness has a dramatic effect on the structural and spectroscopic anisotropy. Simulations with $E_{cc} = 0.6$ kT, $b = 10$ kT rad⁻² reveal two highly ordered but distinct conformations: toroid and rod (Fig. 1)^{8,9,11}. They can be quantitatively identified by the absorption ellipsoid. The simulated H_M curves (Fig. 2) are more similar to the experimental results than are the simulated H_M curves for the random coil and molten globule. The results for the toroid and rod are, however, peaked toward M values higher than experiment and tend to have a narrower distribution. Further insight into the rod and toroid conformations can be obtained by considering a representative simulation trajectory (Fig. 3). For this trajectory, a random-coil

($E_{cc} = 0$, $b = 0$) conformation was chosen as an initial conformation of the simulation, and the parameters were switched to values for a stiff chain with attraction ($E_{cc} = 0.6$ kT, $b = 10$ kT rad⁻²) at the beginning of the simulation. After each 10⁵ steps of the simulation, the instantaneous radius of gyration and absorption cross-sections C_x , C_y and C_z (molecular frame) were calculated. Near the beginning of the simulation, the conformations elongated in response to the increase in chain stiffness, as evidenced by a large R_g . After further Monte Carlo steps, thermal fluctuation produced segment-segment contacts that ‘seeded’ a chain collapse as reflected by the drop in R_g . The instantaneous absorption cross-sections easily allow for the assignment of the chain conformation. Initially, the near equality of the three cross-sections is consistent with the random-coil conformation. Chain collapse to a toroid-like structure is evidenced by one small and two similar, but larger, cross-sections.

One important structural feature that has been left out of existing simulation and theory of stiff polymer chains is chemical defects along the chain. The synthetic procedure for MEH-PPV chains results in chains with 1% or greater tetrahedral rather than conjugated links. Conjugated polymers tend to be reactive, which allows for the further introduction of tetrahedral defects during photoexcitation. In fact, spectroscopic analysis of our MEH-PPV sample leads to a defect concentration estimate of ~5% (ref. 19). We have introduced such chemical defects at random beads in the simulation by tetrahedral bond angles (unchanged force constant). The inclusion of defects has a profound effect on the conformations and their anisotropies. For the case of a stiff chain with defects but no intersegment attraction, an extended conformation is found (V, Fig. 1) with approximately straight chain segments between defects, denoted here as a ‘defect-coil’. The equilibrium structure (not shown) of the same chain without defects is highly extended and considerably more anisotropic. The defect-coil has a lower average anisotropy than the experimental behaviour of MEH-PPV and peaked at lower values.

Structure VI in Fig. 1 is from simulations of stiff chains with defects and intersegment attraction. The simulated anisotropy for this roughly cylindrical conformation is more similar to experiment than any other conformation of Fig. 1. Structure VI, which we denote as a defect-cylinder, is arguably the most accurate representation of the realistic collapsed conformations of conjugated polymers such as MEH-PPV among the idealized structures that have been considered. Indeed, it is unlikely that real conjugated polymer chains, except in special cases, would be sufficiently free of defects to fold into the toroid or rod structures. With respect to the

experimental samples in this study, separate spectroscopic experiments strongly suggest that the spin-coating conditions we use to prepare the samples produce films that contain roughly equal amounts of collapsed and non-collapsed conformations. In fact, an equal superposition of the anisotropy distributions H_M of defect-coil and defect-cylinder (V and VI) is in reasonable agreement with the experimental data. Interestingly, the discovery of highly ordered, cylindrical conformations reported here for MEH-PPV may be a critical factor resolving the puzzling properties of MEH-PPV and related polymers. These include the significant local anisotropy of thin films of pure materials²⁴, and evidence that the structure of MEH-PPV in films can be controlled by the conformation in the solution used to spin-coat the films³⁰. The new conformations introduced in the present work, the defect-coil (V) and defect-cylinder (VI), exhibit a key characteristic, namely, structurally identifiable quasi-straight-chain segments. These segments are therefore excellent candidates for the localized quasi-chromophores in conjugated polymers. These conformations probably also describe other stiff-chain conjugated systems, such as polyfluorene and poly(phenyleneethynylene), that can develop the necessary tetrahedral defects. □

Received 10 February; accepted 5 May 2000.

- de Gennes, P.-G. *Scaling Concepts In Polymer Physics* (Cornell Univ. Press, Ithaca, New York, 1979).
- Grosberg, A. Y. & Kuznetsov, D. V. Quantitative theory of the globule-to-coil transition. *Macromolecules* **25**, 1970–2003 (1992).
- Friend, R. H. *et al.* Electroluminescence in conjugated polymers. *Nature* **397**, 121–128 (1999).
- Hide, F., Diazgarcia, M. A., Schwartz, B. J. & Heeger, A. J. New developments in the photonic applications of conjugated polymers. *Acc. Chem. Res.* **30**, 430–436 (1997).
- Yang, C. Y., Hide, F., Diazgarcia, M. A., Heeger, A. J. & Cao, Y. Microstructure of thin films of photoluminescent semiconducting polymers. *Polymer* **39**, 2299–2304 (1998).
- Bloomfield, V. A. Condensation of DNA by multivalent cations: Consideration on mechanism. *Biopolymers* **31**, 1471–1481 (1991).
- Grosberg, A. Y. Certain possible conformational states of a uniform elastic polymer chain. *Biophysics* **24**, 30–36 (1979).
- Ivanov, V. A., Paul, W. & Binder, K. Finite chain length effects on the coil-globule transition of stiff-chain macromolecules—a Monte Carlo simulation. *J. Chem. Phys.* **109**, 5659–5669 (1998).
- Noguchi, H. & Yoshikawa, K. Morphological variation in a collapsed single homopolymer chain. *J. Chem. Phys.* **109**, 5070–5077 (1998).
- Zhou, Y. Q., Karplus, M., Wichter, J. M. & Hall, C. K. Equilibrium thermodynamics of homopolymers and clusters - molecular dynamics and Monte Carlo simulations of systems with square-well interactions. *J. Chem. Phys.* **107**, 10691–10708 (1997).
- Kuznetsov, Y. A. & Timoshenko, E. G. On the conformational structure of a stiff homopolymer. *J. Chem. Phys.* **111**, 3744–3752 (1999).
- Xie, X. S. & Trautman, J. K. Optical studies of single molecules at room temperature. *Annu. Rev. Phys. Chem.* **49**, 441–480 (1998).
- Basche, T., Moerner, W. E., Orrit, M. & Wild, U. P. (eds) *Single Molecule Optical Detection, Imaging, and Spectroscopy* (Verlag Chemie, Munich, 1996).
- Ha, T., Laurence, T. A., Chemla, D. S. & Weiss, S. Polarization spectroscopy of single fluorescent molecules. *J. Phys. Chem. B* **103**, 6839–6850 (1999).
- Vandenbout, D. A. *et al.* Discrete intensity jumps and intramolecular electronic energy transfer in the spectroscopy of single conjugated polymer molecules. *Science* **277**, 1074–1077 (1997).
- Hu, D., Yu, J. & Barbara, P. F. Single-molecule spectroscopy of the conjugated polymer MEH-PPV. *J. Am. Chem. Soc.* **121**, 6936–6937 (1999).
- Yaliraki, S. N. & Silbey, R. J. Conformational disorder of conjugated polymers—implications for optical properties. *J. Chem. Phys.* **104**, 1245–1253 (1996).
- Gettinger, C. L., Heeger, A. J., Drake, J. M. & Pine, D. J. A photoluminescence study of poly(phenylene vinylene) derivatives—the effect of intrinsic persistence length. *J. Chem. Phys.* **101**, 1673–1678 (1994).
- Padmanaban, G. & Ramakrishnan, S. Conjugation length control in soluble poly[2-methoxy-5-(2'-ethylhexyl)oxy-1,4-phenylenevinylene] (MEHPPV): synthesis, optical properties, and energy migration. *J. Am. Chem. Soc.* **122**, 2244–2251 (2000).
- Mukamel, S., Tretiak, S., Wagersreiter, T. & Chernyak, V. Electronic coherence and collective optical excitations of conjugated molecules. *Science* **277**, 781–787 (1997).
- Woo, H. S. *et al.* Optical spectra and excitations in phenylene vinylene oligomers. *Synth. Met.* **59**, 13–28 (1993).
- Hagler, T. W., Pakbaz, K. & Heeger, A. J. Polarized-electroabsorption spectroscopy of a soluble derivative of poly(p-phenylenevinylene) oriented by gel processing in polyethylene—polarization anisotropy, the off-axis dipole moment, and excited-state delocalization. *Phys. Rev. B* **49**, 10968–10975 (1994).
- Bassler, H. & Schweitzer, B. Site-selective fluorescence spectroscopy of conjugated polymer and oligomers. *Acc. Chem. Res.* **32**, 173–182 (1999).
- Blatchford, J. W. *et al.* Spatially and temporally resolved emission from aggregates in conjugated polymers. *Phys. Rev. B* **54**, R3683–R3686 (1996).
- Thulstrup, E. W. & Michl, J. *Elementary Polarization Spectroscopy* (VCH, New York, 1989).
- Carmesin, I. & Kremer, K. The bond fluctuation method: a new effective algorithm for the dynamics of polymers in all spatial dimensions. *Macromolecules* **21**, 2819–2823 (1988).
- Helfand, E. Theory of the kinetics of conformational transitions in polymer. *J. Chem. Phys.* **54**, 4651–4661 (1971).

- Orion, I., Buisson, J. P. & Lefrant, S. Spectroscopic studies of polaronic and bipolaronic species in n-doped poly(paraphenylenevinylene). *Phys. Rev. B* **57**, 7050–7065 (1998).
- Lodge, T. P. & Fredrickson, G. H. Optical anisotropy of tethered chains. *Macromolecules* **25**, 5643–5650 (1992).
- Nguyen, T. Q., Doan, V. & Schwartz, B. J. Conjugated polymer aggregates in solution: Control of interchain interactions. *J. Chem. Phys.* **110**, 4068–4078 (1999).

Acknowledgements

This work was supported by grants from the National Science Foundation (P.F.B.), the Robert A. Welch Foundation (P.J.R. & P.F.B.), and the Texas Advanced Research Program (P.J.R.). Further support was provided by the Institute for Theoretical Chemistry and by the Laboratory for Spectroscopic Imaging, University of Texas. We also thank A. Yethiraj for discussions.

Correspondence and requests for materials should be addressed to P.F.B. (e-mail: p.barbara@mail.utexas.edu).

Dynamic self-assembly of magnetized, millimetre-sized objects rotating at a liquid–air interface

Bartosz A. Grzybowski*, Howard A. Stone† & George M. Whitesides*

*Harvard University, Department of Chemistry and Chemical Biology, 12 Oxford Street, Cambridge, Massachusetts 02138, USA

†Harvard University, Division of Engineering and Applied Sciences, Pierce Hall, Cambridge, Massachusetts 02138, USA

Spontaneous pattern formation by self-assembly is of long-standing^{1–3} and continuing interest^{4,5} not only for its aesthetic appeal^{6,7}, but also for its fundamental^{8–18} and technological relevance¹⁹. So far, the study of self-organization processes has mainly focused on static structures, but dynamic systems^{20–22}—those that develop order only when dissipating energy—are of particular interest for studying complex behaviour^{23,24}. Here we describe the formation of dynamic patterns of millimetre-sized magnetic disks at a liquid–air interface, subject to a magnetic field produced by a rotating permanent magnet. The disks spin around their axes with angular frequency equal to that of the magnet, and are attracted towards its axis of rotation while repelling each other. This repulsive hydrodynamic interaction is due to fluid motion associated with spinning; the interplay between attractive and repulsive interactions leads to the formation of patterns exhibiting various types of ordering, some of which are entirely new. This versatile system should lead to a better understanding of dynamic self-assembly, while providing a test-bed for stability theories of interacting point vortices^{25–28} and vortex patches²⁹.

We fabricated circular disks by filling hollow polyethylene tubing (~1 mm inside diameter, ~2 mm outside diameter) with poly(dimethylsiloxane) (PDMS) doped with magnetite (~5–30 wt%), and cutting the resulting composite into slices ~400 μm thick. A permanent bar magnet of approximate dimensions ($L \times W \times D$, in cm) $5.6 \times 4 \times 1$ was placed at a distance h (about 2–4 cm) below the interface, and rotated with angular velocity ω (Fig. 1a). The magnet was magnetized along its longest dimension, and had magnetization $M \approx 1,000 \text{ G cm}^{-3}$. When the magnet was stationary, the disks were attracted towards its poles, where they formed orderless aggregates. When the magnet rotated, the disks were drawn towards its axis of rotation. In addition, the magnetic moments of the disks interacted with the rotating magnetic field, and the disks spun around their centres. The fluid motion associated with spinning resulted in a repulsive hydrodynamic

